nature physics

LETTERS

https://doi.org/10.1038/s41567-019-0666-6

Quantum-critical phase from frustrated magnetism in a strongly correlated metal

Hengcan Zhao[1,2], Jiahao Zhang[1,2], Meng Lyu[1,2], Sebastian Bachus[3], Yoshifumi Tokiwa[3], Philipp Gegenwart[3], Shuai Zhang[1,2], Jinguang Cheng[1,2,4], Yi-feng Yang[1,2,4], Genfu Chen[1,2,4], Yosikazu Isikawa[5], Qimiao Si[6]*, Frank Steglich[1,7,8]* and Peijie Sun[1,2,4]*

Strange-metal phenomena often develop at the border of antiferromagnetic order in strongly correlated metals[1]. Previous work established that they can originate from the fluctuations anchored by the quantum-critical point associated with a continuous quantum phase transition out of the antiferromagnetic order[2–4]. What is still unclear is how these phenomena can be associated with a potential new phase of matter at zero temperature. Here, we show that magnetic frustration of the 4*f* local moments in the distorted kagome intermetallic compound cerium palladium aluminium gives rise to such a paramagnetic quantum-critical phase. Our discovery motivates a design principle for strongly correlated metallic states with unconventional excitations.

Geometrical frustration in quantum spin systems gives rise to quantum fluctuations that may suppress long-range magnetic order and cause a quantum spin liquid ground state[5]. Traditionally, this notion was associated with insulating magnets only. More recently, there is increasing recognition that geometrical frustration is also important to bad metals that host local moments, such as strongly correlated *f*-electron metals[6–10], which provide a prototype setting for magnetic quantum phase transitions (QPTs)[2–4,11]. From general theoretical considerations, the magnetic RKKY (Ruderman–Kittel–Kasuya–Yosida) interactions on a geometrically frustrated lattice generate quantum fluctuations that interplay with those produced by the competing Kondo interactions[8–10,12]. The QPT can then involve not only antiferromagnetic order and a paramagnetic heavy Fermi liquid, but also a potential metallic spin liquid phase. Although some have argued that the latter phase may exist in some Kondo systems[6,7,13,14], how it develops from magnetic frustration in a Kondo lattice has not been demonstrated so far.

The distorted kagome lattice system cerium palladium aluminium (CePdAl) with local quantum spins (effective spin $S_{\rm eff}=½$) at temperatures below $T\approx5$ K is well suited for this study[15,16]. Due to geometrical frustration, only two-thirds of these local spins are involved in the magnetic ordering[17], and in the temperature (T)–magnetic field (B) phase diagram the frustration-assisted short-range order sets in at $T_{\rm m}(B)$, substantially above the Néel temperature $T_{\rm N}(B)$ (refs. [16,18]), as shown in Fig. 1a. In the field-induced paramagnetic state, well separated from a first-order antiferromagnetic transition at the highest transition field $B_{\rm cp}\approx4.2$ T, a continuous QPT (or quantum-critical point (QCP)) was identified[18] at $B_0^*\approx4.6$ T; see also Supplementary Fig. 1. At temperature $T=0$ and on increasing the field through B_0^*, a partial delocalization of the 4*f* states takes place, which corresponds to the $T\to0$ extrapolation of a Mott-type (localization–delocalization) cross-over line $B^*(T)$, as introduced in ref. [18]. In addition, B_0^* is the $T\to0$ terminating point of two other cross-over lines, one into a Fermi liquid phase at $B>B_0^*$, and the other into a frustration-assisted metallic spin liquid state at $B_{\rm cp}<B<B_0^*$. At $B=B_0^*$, about 75% of the magnetization is already saturated[19]. In contrast to the behaviour of other antiferromagnetic Kondo systems[13,14], non-Fermi liquid (NFL) phenomena reflecting quantum criticality could not be observed for CePdAl in the electrical resistivity, ρ, in the paramagnetic low-temperature phase near B_0^*. This was ascribed to the large Zeeman splitting of the crystal-field ground-state doublet of the cerium 4*f* shell, which causes a correspondingly large reduction of spin flip scattering and an enhanced temperature dependence of the resistivity[18].

To avoid the effect of Zeeman splitting, here, we study CePdAl at hydrostatic pressure, p, up to about 2 GPa, using a single crystal from the same batch as employed in ref. [18]. In cerium-based heavy-fermion systems, pressure is known to enhance the Kondo coupling between the 4*f* and conduction electrons and to weaken the magnetic order. Therefore, the magnetic QPT can be studied by the pressure alone or in combination with a lower magnetic field and, thus, at a smaller ratio of the Zeeman splitting to the Kondo energy. As a result, the NFL phenomena related to quantum criticality may eventually become fully resolved through measurements such as of the electrical resistivity as a function of temperature. Two immediate questions arise: (1) will signatures for Mott-type—called Kondo destruction—quantum criticality[20,21] be observed even at elevated pressures, and if so, (2) to what extent is the Kondo-destruction quantum criticality intertwined with the magnetic frustration?

The T–p phase diagram at zero magnetic field is shown in Fig. 1a. Hydrostatic pressure suppresses the antiferromagnetic order in CePdAl at the lower critical pressure $p_{\rm c1}\approx0.9$ GPa, as reported in ref. [19]. We observe a funnel regime with linear temperature dependence of the resistivity that terminates at $T\approx0.3$ K. At lower temperatures, the system enters a regime associated with the quantum-critical phase. NFL behaviour exists over a finite pressure range between $p=p_{\rm c1}$ and the upper critical pressure $p_{\rm c2}\approx1.7$ GPa. Here, the temperature dependence of the electrical resistivity follows a power law, $\Delta\rho(T)=\rho(T)-\rho_0=A'T^n$, where ρ_0 is the residual resistivity

[1]Beijing National Laboratory for Condensed Matter Physics, Institute of Physics, Chinese Academy of Sciences, Beijing, China. [2]School of Physical Sciences, University of Chinese Academy of Sciences, Beijing, China. [3]Experimental Physics VI, Center for Electronic Correlations and Magnetism, Institute of Physics, University of Augsburg, Augsburg, Germany. [4]Songshan Lake Materials Laboratory, Dongguan, China. [5]Graduate School of Science and Engineering, University of Toyama, Toyama, Japan. [6]Department of Physics and Astronomy, Rice Center for Quantum Materials, Rice University, Houston, TX, USA. [7]Max Planck Institute for Chemical Physics of Solids, Dresden, Germany. [8]Center for Correlated Matter, Zhejiang University, Hangzhou, China. *e-mail: qmsi@rice.edu; steglich@cpfs.mpg.de; pjsun@iphy.ac.cn

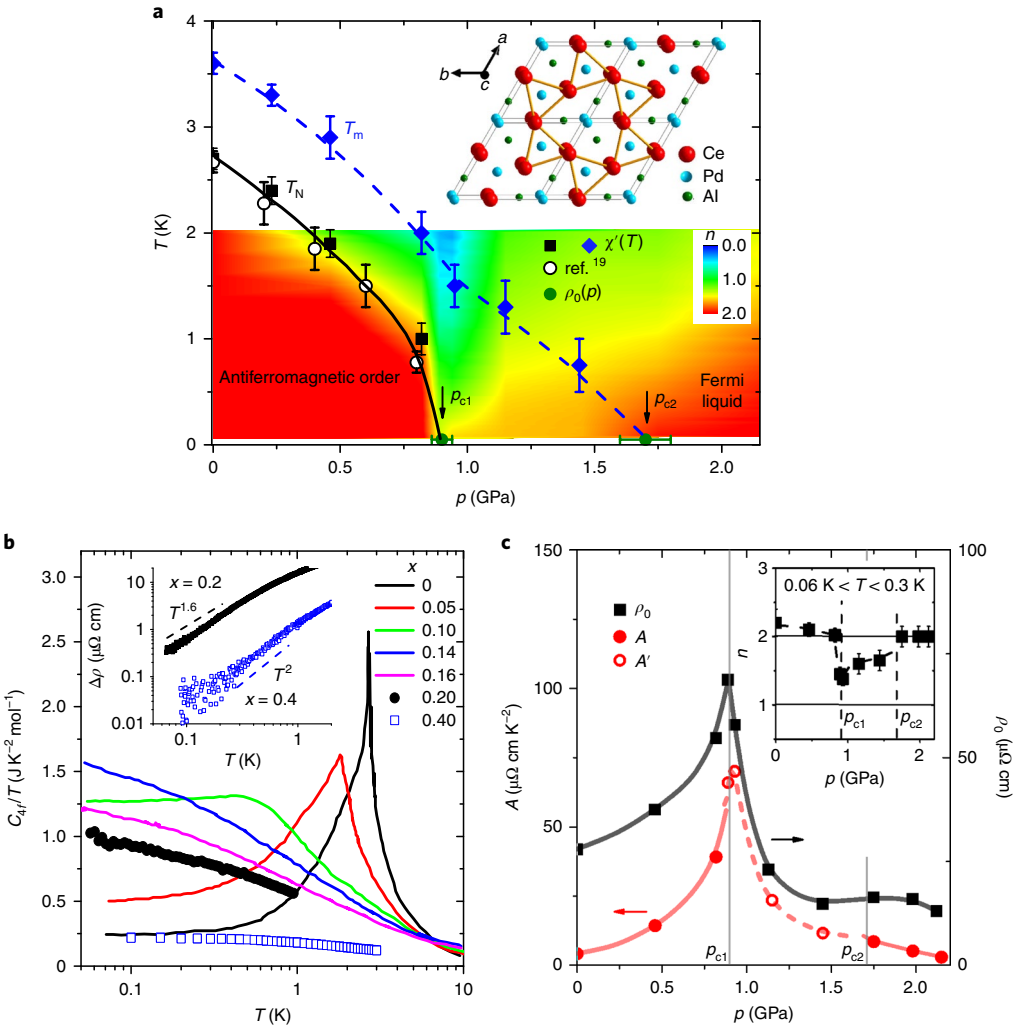

Fig. 1 | Results at zero field illustrating the emerging quantum-critical phase. a, T–p phase diagram for $B=0$ on top of a colour-coded map for the exponent n of $\Delta\rho(T) \propto T^n$. T_N and T_m are derived from the inflection points and maxima, respectively, of the (real part of the) $\chi'(T)$ curves, shown in Supplementary Fig. 2b. Open circles mark the Néel temperatures derived from the d.c. susceptibility measurements from ref. [19]. Error bars reflect the standard deviations in determining T_N and T_m from the a.c./d.c. susceptibility data (see Supplementary Fig. 2b,c). The phase space at $T>2$ K is left white because $\rho(T)$ was typically measured only up to 2 K in a dilution fridge. Inset: a sketch of the distorted kagome lattice of CePdAl. **b**, C_{4f}/T as a function of T for $CePd_{1-x}Ni_xAl$ with x up to 0.4. The data for $x=0.2$ and $x=0.4$, which are beyond the critical concentration $x\approx0.144$ (ref. [23]), were determined in this work, while the other curves are reproduced from ref. [24]. For $x=0.2$, a logarithmic increase of $C_{4f}(T)/T$ exists down to 0.06 K. In contrast, we find a flat and large $C_{4f}(T)/T$ below 0.5 K for $x=0.4$. This indicates heavy Fermi liquid behaviour, as documented by the large size of $C_{4f}(T)/T$ at low temperatures. Inset: $\Delta\rho$ versus T in a double-log scale; here, we observe $\Delta\rho \propto T^{1.6}$ for $x=0.2$ and $\Delta\rho \propto T^2$ for $x=0.4$. **c**, A and A' in $\Delta\rho(T) \propto T^n$, with $n=2$ and $n<2$, respectively, as well as ρ_0 as a function of p. The large size of A provides evidence for a heavy Fermi liquid phase. Inset: n versus p estimated at the lowest temperatures (0.06–0.3 K). Note that $n\approx1.4$ at p_{c1} and that the Fermi liquid behaviour with $n=2$ is restored at $p>p_{c2}$. Error bars of the n values represent standard errors of the fits to $\rho(T)$.

and A' is a coefficient, and with the exponent n being smaller than the Fermi liquid value $n=2$ (see inset of Fig. 1c and Supplementary Fig. 2a, as well as the colour code in Fig. 1a). The upper cut-off, $T_m(p)$, of this NFL regime is smoothly connected to the cross-over line $T_m(B)$ at lower pressure; measurements of magnetoresistivity[18] and entropy[16] at ambient pressure have implicated $T_m(B)$ as the onset of frustration-assisted short-range order in a paramagnetic phase akin to a spin liquid, in which the RKKY interactions have dynamically suppressed the Kondo singlet formation (compare with the paramagnetic phase with a small Fermi surface, P_S, of Fig. 4b). The cross-over scale $T_m(p)$ vanishes at $p=p_{c2}$. A Fermi-liquid-like temperature dependence of the resistivity, $\Delta\rho(T)=AT^2$, with a large value for the coefficient A, is observed in the antiferromagnetically ordered regime $p<p_{c1}$, similar to what was found in the antiferromagnetic low-field phase of $YbRh_2Si_2$ (ref. [22]), as well as at $p>p_{c2}$.

The specific heat of nickel-substituted CePdAl at ambient pressure provides additional evidence beyond the resistivity for this quantum-critical phase. Figure 1b shows the 4f-derived specific heat, presented as C_{4f}/T versus T, for $Ce(Pd_{1-x}Ni_x)Al$ single crystals, with x varying between 0 and 0.4. Nickel substitution for palladium was previously shown to act as chemical pressure[23], where a critical nickel concentration of $x_{c1}=0.144$ corresponds to p_{c1}, and assuming a linear relationship, we expect that $x_{c2}\approx0.27$ will correspond to p_{c2}. With a small amount of nickel substitution, the magnetic phase-transition anomaly is rapidly broadened and shifted to lower temperatures[24]. For $x=0.2$, which lies between x_{c1} and x_{c2}, an NFL-like, divergent temperature dependence is seen in $C_{4f}(T)/T$, in line

with the corresponding $\rho(T)$ curve that reveals a $T^{1.6}$ dependence below about 0.5 K (inset of Fig. 1b). For $x=0.4$, which is much larger than x_{c2}, $C_{4f}(T)/T$ saturates below about 0.3 K, and we observe a T^2 dependence of the resistivity at $T<0.8$ K (inset of Fig. 1b). The zero-temperature values of $C_{4f}(T)/T$, extrapolated from the measured low-temperature data, vary between 0.25 J K^{-2} mol^{-1} and more than 1.5 J K^{-2} mol^{-1}, illustrating heavy fermion behaviour.

To further characterize the NFL phase, we show the pressure dependence of A and A' of the power laws $\Delta\rho(T)=AT^2$ and $A'T^n$ ($n<2$) and the residual resistivity at $B=0$ for pure CePdAl in Fig. 1c. All three quantities exhibit a sharp peak at p_{c1}, where the resistivity exponent becomes smallest ($n\approx1.4$); n, which is 2 in the antiferromagnetic phase, shows a relatively sharp decrease for $p\geq p_{c1}$ and reaches 2 again close to p_{c2} (see inset of Fig. 1c). In contrast to p_{c1}, p_{c2} can be identified from only a very weak anomaly, for example, a small and broadened hump in $\rho_0(B)$.

In Fig. 2, we plot the temperature dependence of the zero-field resistivity between 0.06 K and 1.5 K for three different pressure values in the NFL phase (see also Supplementary Fig. 2a). These results reveal an increasing 'quantum-critical strength' on releasing the pressure inside this phase. Specifically, the apparent linear temperature dependence of $\rho(T)$ found at elevated temperatures turns into a power-law behaviour, $\Delta\rho(T)\propto T^n$, $1<n<2$, in the low-temperature regime: the cross-over temperature decreases when pressure decreases, so on the approach to the QCP at $p_{c1}\approx0.9$ GPa. At the same time, the exponent n decreases from 1.7 (1.44 GPa) to 1.6 (1.15 GPa) and reaches the critical value $n=1.4$ (0.93 GPa) slightly above p_{c1}. A corresponding trend is seen in the specific-heat results of the CePdAl samples with nickel substitution $x=0.2$ and $x=0.14$, respectively, presented in Supplementary Fig. 3a. Here, $C_{4f}(T)/T$ follows a $-\ln T$ dependence at elevated temperatures and crosses over to a weaker increase at lower temperatures: again, the cross-over temperature decreases when approaching the critical concentration $x=0.144$. The existence of these unusual transport and thermodynamic properties over an extended range of pressure provides a notably high level of evidence and characterization for a quantum-critical phase in a frustrated heavy-fermion metal. Compared with heavy-fermion/organic metals without apparent geometrical frustration, where this type of phase has been implicated[13,14,25,26], the frustrated geometry of the crystalline lattice in CePdAl apparently facilitates the quantum-critical phase in the continuous evolution of low-temperature singularities of both transport and thermodynamic properties.

In addition to bringing about a quantum-critical phase, the geometrically frustrated nature of CePdAl provides the opportunity to elucidate its interplay with the Kondo coupling. To do so, it is necessary to tune the system by more than one control parameter. Field tuning at ambient pressure[15,16,18] provides further motivation, so we study the combined effect of pressure and magnetic field. Importantly, under pressure, the increased Kondo coupling will enhance the 'Kondo broadening' (see Supplementary Fig. 9 and related discussion) of the Zeeman states and diminish the effect of Zeeman splitting on the measured dependence of the resistivity on the temperature. This reveals the true NFL behaviour. For the finite field $B=2$ T, we show $\rho(T)$ curves measured for varying p and the corresponding T–p phase diagram in Fig. 3a,c, respectively; the latter is qualitatively similar to that for $B=0$ in Fig. 1a. In contrast to the NFL-type T^n dependence of the resistivity with $1.4<n<2$ over a greatly extended pressure range of 0.9–1.7 GPa (that is, p_{c1}–p_{c2}) for $B=0$, a low-temperature power law with $n=1\pm0.1$ is observed for $B=2$ T within the range 0.8 GPa $<p<$ 1.0 GPa, a much reduced pressure window.

In addition, we show $\rho(T)$ curves measured for varying B and the corresponding T–B phase diagram for $p=0.82$ GPa, slightly below p_{c1}, in Fig. 3b,d. When compared with the corresponding phase diagram at ambient pressure (see fig. 2 in ref. [18]), the most striking difference is an exponent $n=1\pm0.1$ in the power-law temperature

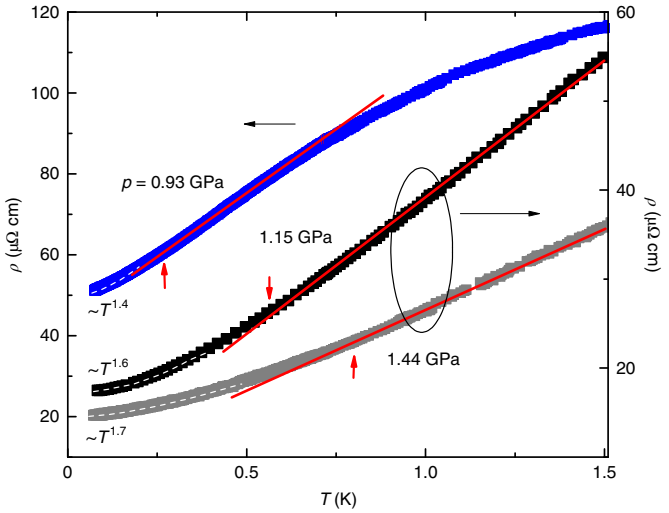

Fig. 2 | Pressure dependence of $\rho(T, B=0)$ as a measure of the quantum-critical strength within the quantum-critical phase. For all of the three pressures ($p=0.93$ GPa, 1.15 GPa and 1.44 GPa) within the quantum-critical phase, we observe a linear-in-temperature resistivity at elevated temperatures (red solid lines); below a cross-over temperature T_f (marked by red arrows), at which the system enters a regime associated with the low-temperature quantum-critical phase, $\Delta\rho(T)$ changes to be proportional to T^n ($1<n<2$) (white dashed lines). Both n values and the cross-over temperature decrease on lowering the pressure, indicating an increasing quantum-critical strength. Note that for $p=0.93$ (close to p_{c1}, left scale), the intermediate temperature range, where $\Delta\rho(T)\propto T$, is substantially limited at the high-temperature side by the combined action of Kondo lattice coherence and notable antiferromagnetic short-range correlations that become visible at $T>1$ K (see Supplementary Information). The curves for $p=1.15$ GPa and 1.44 GPa are referring to the right scale. The same data are also shown in Supplementary Fig. 3b as a function of T^2.

dependence of $\rho(T)$ at $B=3$ T (see Supplementary Fig. 6c), at which field this almost linear temperature dependence is observed from 0.4 K all the way down to $T\approx0.06$ K, the lowest accessible temperature. Such a nearly temperature-linear resistivity extends to about $B_0^*\approx3.5$ T (see Fig. 3b). In contrast, no NFL behaviour ($n<2$) could be resolved at $p=0$ (ref. [18]), as mentioned in the introduction. As is clearly seen in Fig. 3b,d, at $B>B_0^*$, the apparent quadratic temperature dependence of $\rho(T)$ indicates a Fermi liquid phase.

In the following, we discuss results that highlight the existence of a $B_0^*(p)$ line at which the 4f electrons delocalize in the zero-temperature limit[20,21,27–29]. Figure 3e shows the evolution of the coefficient A of the T^2 dependence of the resistivity as a function of the magnetic field near and above p_{c1}. For $p=0.82$ GPa, there is a strong increase from both the antiferromagnetic and paramagnetic side, suggesting a potential divergence of $A(B)$ at a Kondo-destroying antiferromagnetic QCP, $B_0^*(p=0.82\text{ GPa})\approx3.5$ T. Note that for this pressure, the resistivity exhibits an almost linear temperature dependence of $\rho(T)$ between $B=3$ T and $B=3.5$ T to the lowest temperature, as mentioned above (see Fig. 3b). Likewise, a temperature-linear $\rho(T)$ is also observed at $B_0^*(p=0.93\text{ GPa})\approx2$ T (see Fig. 3a,c). These values of $B_0^*(p)$ are in reasonable agreement with the ones read off the $B_0^*(p)$ curve in the inset of Supplementary Fig. 5a, as derived from the inflection points/maxima in $\chi'(B)$, where χ' is the real part of the a.c. susceptibility, measured at fixed pressure values and registered at $T=0.08$ K (compare with the arrows in Supplementary Fig. 5a). At 0.93 GPa $<p<p_{c2}$, the resistivity shows NFL behaviour at low fields (see Fig. 1a and 4a), but follows a T^2 law at fields that are sufficiently larger than $B_0^*(p)$. In these higher fields, we still observe an increase of $A(B)$ when the field decreases, and this increase

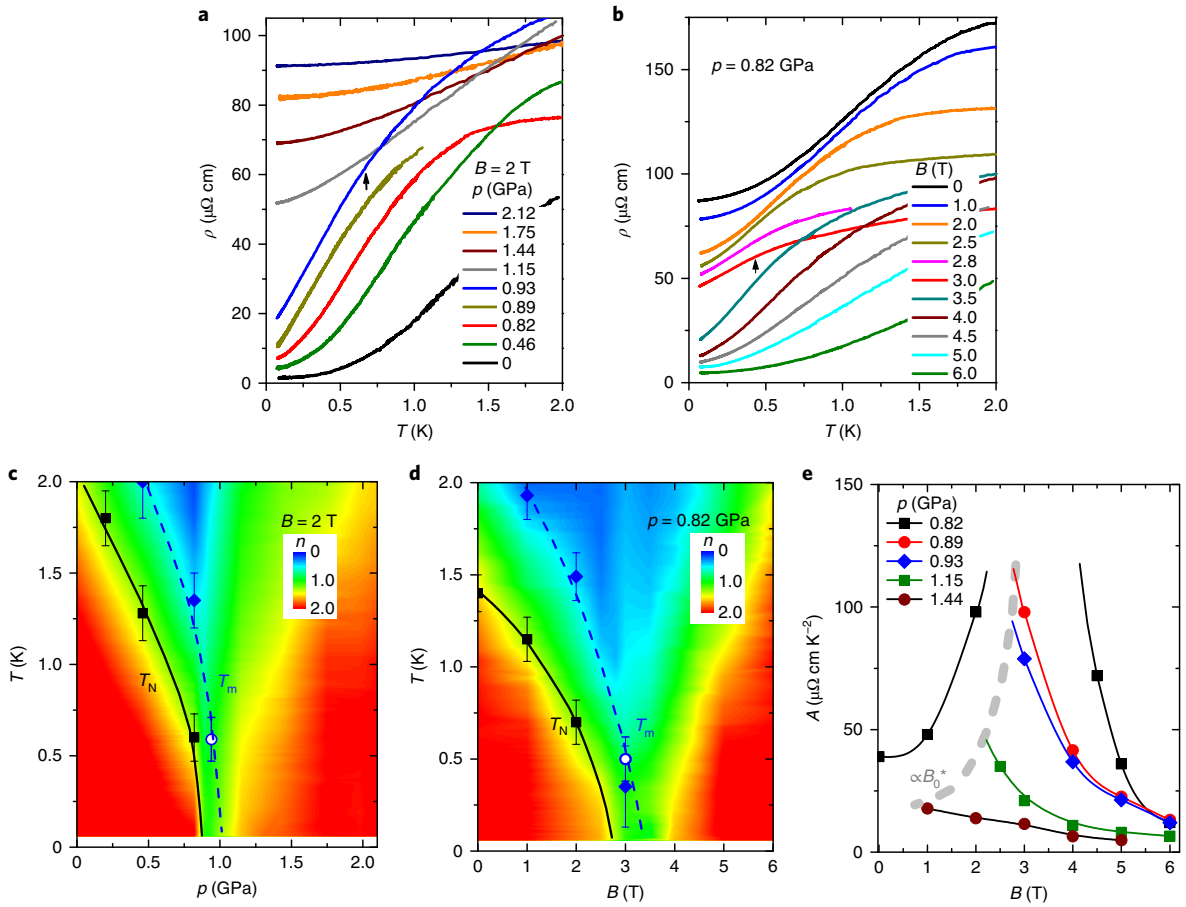

Fig. 3 | NFL behaviour studied at combined control parameters of magnetic field and hydrostatic pressure. a,**b**, $\rho(T)$ curves measured at finite field ($B=2$ T) for various pressures (**a**) and at finite pressure ($p=0.82$ GPa) for various fields (**b**). Best linear-in-temperature resistivity is observed for $p=0.93$ GPa in **a** and $B=3.0$ T in **b**, below the temperature marked by an arrow. **c**, *T*–*p* phase diagram at $B=2$ T. NFL behaviour characterized by an almost linear-in-temperature resistivity exists between the $T_N(p)$ and $T_m(p)$ lines, as evidenced by the green coding in the *n* map. **d**, *T*–*B* phase diagram at $p=0.82$ GPa. Similar to **c**, here, NFL is also observed between the $T_N(p)$ and $T_m(p)$ lines. Error bars denote the standard deviations in determining the values of T_N and T_m from the susceptibility data. This is to be compared with the complex *T*–*B* phase diagram at ambient pressure, where multiple first-order metamagnetic transitions appear, but NFL is absent[18]. The temperature indicated by an arrow in **a** and **b** falls, within the error bar, on the $T_m(p)$ and $T_m(B)$ lines in **c** and **d** (open circles), respectively. The colour-coded *n* maps in **c** and **d** are generated from the $\rho(T)$ curves shown in **a** and **b**, respectively. **e**, The coefficient *A* estimated from the Fermi liquid T^2 dependence of $\rho(T)$ as a function of *B* for different pressures. For $p=0.82$ GPa, an incipient divergence of $A(B)$ is observed below and above $B_0^*\approx3.5$ T. For both $p=0.89$ GPa and 0.93 GPa (close to p_{c1}), a divergence of $A(B)$ towards B_0^* from the paramagnetic side may still be anticipated. At higher pressures, NFL behaviour is found on the low-field side. However, $\rho(T)$ exhibits a T^2 dependence sufficiently above $B=B_0^*(p)$. Here, the field where $A(B, p=\text{constant})$ takes the largest value decreases with increasing pressure and vanishes at $p\approx p_{c2}$. The dashed grey line indicating the locations of these largest *A* coefficients is in good agreement with $B_0^*(p)$ as derived independently from other probes (see main text).

becomes continuously weaker and extends to lower cross-over fields $B_0^*(p)$ when the pressure increases (see Fig. 3e)—again illustrating that inside the quantum-critical phase, the quantum-critical singularity becomes more pronounced on decreasing pressure.

We can now put together the combined pressure and field tunings into the zero-temperature phase diagram shown in Fig. 4a. Here, the colour code illustrates the exponent of the low-temperature power-law dependence of $\rho(T)$ at fields only at which the Zeeman splitting can be neglected (see Supplementary Fig. 9 and the related discussion). Most strikingly, this $T=0$ *p*–*B* phase diagram reveals a quantum-critical phase between the 'Mott line' (a line of true QPTs from $B_0^*(0)$ up to $B_0^*(p_{c1})\approx2.5$ T that turns into a line of quantum cross-overs at higher pressures) and the line of antiferromagnetic QPTs. The Mott line contains several segments. The first segment goes from ambient pressure to about $p=0.3$ GPa, where, most likely, a line of continuous QPTs or QCPs exists (see Supplementary Information). The second segment goes from $p=0.8$ GPa to slightly below $p=1$ GPa, where the temperature-linear resistivity persists to the lowest temperatures (Supplementary Fig. 6c) and the coefficient *A* of the T^2 resistivity component diverges as the line is approached from both sides (see Fig. 3e). Both of these observations implicate the continuation of the line of QCPs from the low-pressure part. Finally, for pressures from $p\approx1$ GPa to the terminating pressure ($p_{c2}\approx1.7$ GPa) of the line, the third segment corresponds to a cross-over that separates the NFL ($\Delta\rho(T)\propto T^n$, $n<2$) and Fermi liquid ($\Delta\rho(T)\propto T^2$) regimes. This is shown by the colour code in Fig. 4a and where the coefficient *A* of the T^2 term in $\rho(T)$ is maximized but does not diverge (Fig. 3e). Across the Mott line, even though measurements of angle-resolved photoemission or quantum oscillations are essentially impossible because of the low temperature and the finite but not sufficiently large magnetic fields involved, a jump in the Fermi surface across the first segment is evidenced by the combined magneto-transport and magnetic susceptibility measurements at ambient[18] as well as finite but relatively small pressure (see

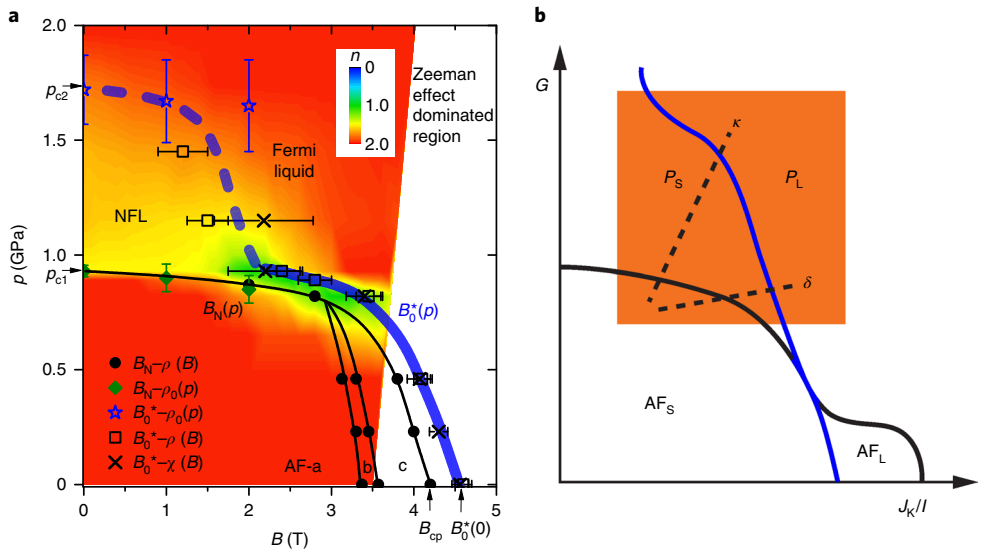

Fig. 4 | Experimental *p*–*B* and schematic global *G*–J_K/I phase diagrams at zero temperature. a, *p*–*B* phase diagram for magnetically frustrated CePdAl at $T=0$ with QPTs (solid lines) and cross-over (dashed thick line) as extrapolated from finite temperature results. The colour code for fields below approximately 3.5 T ($p=0$) and 3.7 T ($p=0.82$ GPa), where the Zeeman effect is negligible (see Supplementary Information), indicates the exponent n in $\Delta\rho(T) \propto T^n$. In addition to the antiferromagnetic phase boundary $B_N(p)$ at fields below 3 T, at higher fields, there are metamagnetic phase boundaries between three antiferromagnetic phases, AF-a, AF-b, AF-c, as well as the boundary to the paramagnetic phase, terminating ($T \to 0$) at B_{cp} (ref. [18]). All magnetic phase boundaries seem to merge at a potential multicritical point near 0.8 GPa and 3 T. The existence range of antiferromagnetism is embraced by the Mott line, where the solid blue line shows the true QPTs from $B_0^*(0)$ up to $B_0^*(p_{c1}) \approx 2.5$ T, and the dashed blue line shows the quantum cross-overs. It separates the itinerant, heavy Fermi liquid, regime in the upper-right part of the phase diagram from the local-moment paramagnetic and antiferromagnetic regimes in the lower-left part. Error bars denote the standard deviations in field or pressure when determining $B_N(p)$ and $B_0^*(p)$ (see Supplementary Figs. 4 and 5). **b**, Global phase diagram ($T=0$) in the parameter space of quantum fluctuations of G and J_K/I. We propose that the shaded region contains the qualitative projection of the combined *p*–*B* tunings of **a** onto the G–J_K/I plane (see main text). The parameter G, like J_K and I, is specified at the Hamiltonian level and therefore well defined for a Kondo lattice model, regardless of whether the ground state is in the Kondo-screened or local-moment regime. The black line denotes transitions between AF and paramagnetic (P) phases, while the blue line specifies Kondo-destruction transitions between phases with large (L) and small (S) Fermi surfaces. The paramagnetic phase whose Fermi surface is large (from Kondo entanglement) is denoted by P_L, and the antiferromagnetic counterparts of P_L and P_S are labelled AF_L and AF_S, respectively. The cut κ captures the effect of the pressure tuning (see Figs. 1a and 3a,c and Supplementary Fig. 2a), while the cut δ of the magnetic-field tuning is based on Fig. 3b,d.

Supplementary Information). By continuity, we conjecture that this jump continues up to and across the second segment of the Mott line. For the antiferromagnetic QPTs at $p \simeq 0.8$ GPa and $B \simeq 3$ T, an antiferromagnetic multicritical point may probably be observed in future studies; for fields below this point, the antiferromagnetic transition is continuous, while for fields above it, the metamagnetic transitions are of first order[16,18]. Finally, it is intriguing to observe the magnetically ordered phases of CePdAl to show heavy Fermi liquid behaviour, similar to the case of $YbRh_2Si_2$ (ref. [22]).

Our results can be viewed from the perspective of a ($T=0$) 'global' phase diagram[8–10,30] (Fig. 4b), which is specified in terms of two quantities: the ratio of the Kondo interaction (J_K) to the RKKY interaction (I), and the degree of quantum fluctuations of the local-moment magnetism (G). The tuning parameters pressure and magnetic field do not affect the geometrical frustration of the distorted kagome lattice that dictates a large value of G. However, they modify the magnetic frustration and further tune G by changing the effective range of the RKKY interaction, while also varying the J_K/I ratio. This means that the application of pressure and field, which are non-universal quantities, results in two different cuts, denoted by κ and δ, within the orange part of the global phase diagram. We can then qualitatively project the tunings in the *p*–*B* plane of Fig. 4a onto the G–J_K/I plane of Fig. 4b and interpret the observed NFL phase between these cuts in terms of the frustration-induced P_S phase with Kondo destruction[20,21,27–29,31]. This implies another notable finding, namely that the observed transition from the magnetic order to the paramagnetic NFL phase represents an unusual type of metallic antiferromagnetic QCP of the local moments. Here, the local moments are Kondo-coupled to the conduction electrons at the Hamiltonian level, but the ground state on either side of the transition is Kondo-destroyed. This type of quantum criticality, although inherent to the proposed global phase diagram, has previously been difficult to observe[32]. Whether or not measurements at even lower temperatures can isolate the singularities associated with this QCP from those of the NFL phase associated with the Mott line is an intriguing open question for future studies. In addition, whether or not further theoretical studies[33,34] can demonstrate the continuation of a line of zero-temperature delocalization–localization (Kondo destruction) phase transition into a line of cross-over (Fig. 4a) is an important problem raised by our study.

Our results demonstrate geometrical frustration as a means of creating strange metals, whose unusual electronic excitations underlie the exotic properties of high-temperature cuprate superconductors[35], organic charge-transfer salts[26] and a variety of other strongly correlated quantum materials[1].

Online content

Any methods, additional references, Nature Research reporting summaries, source data, statements of code and data availability and associated accession codes are available at https://doi.org/10.1038/s41567-019-0666-6.

Received: 29 December 2018; Accepted: 13 August 2019;
Published online: 30 September 2019

References

1. Keimer, B. & Moore, J. E. The physics of quantum materials. *Nat. Phys.* **13**, 1045–1055 (2017).
2. Coleman, P. & Schofield, A. Quantum criticality. *Nature* **433**, 226–229 (2005).
3. von Lőhneysen, H., Rosch, A., Vojta, M. & Wőlfle, P. Fermi-liquid instabilities at magnetic quantum phase transitions. *Rev. Mod. Phys.* **79**, 1015–1075 (2007).
4. Gegenwart, P., Si, Q. & Steglich, F. Quantum criticality in heavy-fermion metals. *Nat. Phys.* **4**, 186–197 (2008).
5. Balents, L. Spin liquids in frustrated magnets. *Nature* **464**, 199–208 (2010).
6. Tokiwa, Y., Ishikawa, J. J., Nakatsuji, S. & Gegenwart, P. Quantum criticality in a metallic spin liquid. *Nat. Mater.* **13**, 356–359 (2014).
7. Tokiwa, Y., Stingl, C., Kim, M.-S., Takabatake, T. & Gegenwart, P. Characteristic signatures of quantum criticality driven by geometrical frustration. *Sci. Adv.* **1**, e1500001 (2015).
8. Si, Q. Global magnetic phase diagram and local quantum criticality in heavy fermion metals. *Phys. B* **378–380**, 23–27 (2006).
9. Si, Q. Quantum criticality and global phase diagram of magnetic heavy fermions. *Phys. Stat. Sol. B* **247**, 476–484 (2010).
10. Coleman, P. & Nevidomskyy, A. H. Frustration and the Kondo effect in heavy fermion materials. *J. Low Temp. Phys.* **161**, 182–202 (2010).
11. Stewart, G. R. Non-Fermi-liquid behavior in *d*- and *f*-electron metals. *Rev. Mod. Phys.* **73**, 797–855 (2001).
12. Doniach, S. Kondo lattice and weak antiferromagnetism. *Phys. B* **91**, 231–234 (1977).
13. Friedemann, S. et al. Detaching the antiferromagnetic quantum critical point from the Fermi-surface reconstruction in $YbRh_2Si_2$. *Nat. Phys.* **5**, 465–469 (2009).
14. Custers, J. et al. Evidence for a non-Fermi-liquid phase in Ge-substituted $YbRh_2Si_2$. *Phys. Rev. Lett.* **104**, 186402 (2010).
15. Zhao, H. C. et al. Temperature-field phase diagram of geometrically frustrated CePdAl. *Phys. Rev. B* **94**, 235131 (2016).
16. Lucas, S. et al. Entropy evolution in the magnetic phases of partially frustrated CePdAl. *Phys. Rev. Lett.* **118**, 107204 (2017).
17. Dolores Núñez-Regueiro, M., Lacroix, C. & Canals, B. Magnetic ordering in the frustrated Kondo lattice compound CePdAl. *Phys. C* **282–287**, 1885–1886 (1997).
18. Zhang, J. H. et al. Kondo destruction in a quantum paramagnet with magnetic frustration. *Phys. Rev. B* **97**, 235117 (2018).
19. Goto, T., Hane, S., Umeo, K., Takabatake, T. & Isikawa, Y. Field-induced magnetic transitions and pressure-induced magnetic instability in CePdAl. *J. Phys. Chem. Solids* **63**, 1159–1163 (2002).
20. Si, Q., Rabello, S., Ingersent, K. & Smith, J. L. Locally critical quantum phase transitions in strongly correlated metals. *Nature* **413**, 804–808 (2001).
21. Coleman, P., Pepin, C., Si, Q. & Ramazashvili, R. How do Fermi liquids get heavy and die? *J. Phys. Condens. Matter* **13**, 723–738 (2001).
22. Gegenwart, P. et al. Magnetic-field induced quantum critical point in $YbRh_2Si_2$. *Phys. Rev. Lett.* **89**, 056402 (2002).
23. Fritsch, V. et al. Approaching quantum criticality in a partially geometrically frustrated heavy-fermion metal. *Phys. Rev. B* **89**, 054416 (2014).
24. Sakai, A. et al. Signature of frustrated moments in quantum critical $CePd_{1-x}Ni_xAl$. *Phys. Rev. B* **94**, 220405 (2016).
25. Tomita, T., Kuga, K., Uwatoko, Y., Coleman, P. & Nakatsuji, S. Strange metal without magnetic criticality. *Science* **349**, 506–509 (2015).
26. Oike, H., Miyagawa, K., Taniguchi, H. & Kanoda, K. Pressure-induced Mott transition in an organic superconductor with a finite doping level. *Phys. Rev. Lett.* **114**, 067002 (2015).
27. Paschen, S. et al. Hall-effect evolution across a heavy-fermion quantum critical point. *Nature* **432**, 881–885 (2004).
28. Gegenwart, P. et al. Multiple energy scales at a quantum critical point. *Science* **315**, 969–971 (2007).
29. Friedemann, S. et al. Fermi-surface collapse and dynamical scaling near a quantum-critical point. *Proc. Natl Acad. Sci. USA* **107**, 14547–14551 (2010).
30. Custers, J. et al. Destruction of the Kondo effect in the cubic heavy-fermion compound $Ce_3Pd_{20}Si_6$. *Nat. Mater.* **11**, 189–194 (2012).
31. Senthil, T., Vojta, M. & Sachdev, S. Weak magnetism and non-Fermi liquids near heavy-fermion critical points. *Phys. Rev. B* **69**, 035111 (2004).
32. Küchler, R. et al. Uniaxial stress tuning of geometrical frustration in a Kondo lattice. *Phys. Rev. B* **96**, 241110 (2017).
33. Pixley, J. H., Yu, R. & Si, Q. Quantum phases of the Shastry–Sutherland Kondo lattice: implications for the global phase diagram of heavy-fermion metals. *Phys. Rev. Lett.* **113**, 176402 (2014).
34. Ramires, A. & Coleman, P. Supersymmetric approach to heavy fermion systems. *Phys. Rev. B* **93**, 035120 (2016).
35. Lee, P. A., Nagaosa, N. & Wen, X.-G. Doping a Mott insulator: physics of high-temperature superconductivity. *Rev. Mod. Phys.* **78**, 17–85 (2006).

Acknowledgements

This work was supported by the Ministry of Science and Technology of China (grant nos 2017YFA0303100, 2015CB921303 and 2018YFA0305702), the National Natural Science Foundation of China (grant nos 11774404, 11474332, 11574377 and 11874400), the Chinese Academy of Sciences (grant nos XDB07020200, XDB25000000 and QYZDB-SSW-SLH013) and a fund from the Science and Technology on Surface Physics and Chemistry Laboratory (no. 01040117). Work at Augsburg was supported by the German Research Foundation (DFG) under the auspices of TRR 80 (no. 107745057), while work at Dresden was partly supported by the DFG Research Unit 960. The work at Rice University was supported in part by the NSF grant DMR-1920740 and the Robert A. Welch Foundation grant C-1411. Q.S. acknowledges the hospitality and support by a Ulam Scholarship from the Center for Nonlinear Studies at Los Alamos National Laboratory and the hospitality of the Aspen Center for Physics (NSF, PHY-1607611).

Author contributions

P.S. and F.S. initiated the project; H.Z., J.Z., M.L. and P.S. performed the transport and susceptibility measurements under pressure; S.B., Y.T., P.G., S.Z. and G.C. performed the heat capacity measurements; J.C. calibrated the pressure cell and performed preliminary transport measurements under pressure; Y.I. prepared and oriented the single crystals; H.Z., J.Z., Y.Y., Q.S., F.S. and P.S. discussed the results and analysed the data; P.S., F.S. and Q.S. wrote the manuscript; all authors revised and approved the manuscript.

Competing interests

The authors declare no competing interests.

Additional information

Supplementary information is available for this paper at https://doi.org/10.1038/s41567-019-0666-6.

Correspondence and requests for materials should be addressed to Q.S., F.S. or P.S.

Peer review information *Nature Physics* thanks Kazushi Kanoda, Gregory Stewart and the other, anonymous, reviewer(s) for their contribution to the peer review of this work.

Reprints and permissions information is available at www.nature.com/reprints.

Publisher's note Springer Nature remains neutral with regard to jurisdictional claims in published maps and institutional affiliations.

Methods

Single crystals of CePdAl and its nickel-doped homologues were prepared by the Czochralski method in an argon gas atmosphere of 5 torr using a tungsten crucible in an induction furnace[15]. The samples were oriented by the Laue backscattering and/or X-ray diffraction method, and then cut into bar shapes by a precision diamond wire saw. For all of the measurements in this work, the electrical current was applied perpendicular to the *c* axis and the magnetic field parallel to the *c* axis, which is the Ising-like, easy magnetic axis. To produce hydrostatic pressures, we used a self-clamped piston-cylinder pressure cell made of non-magnetic CuBe and NiCrAl, with glycerol as the pressure-transmitting medium. The generated pressure was monitored by the superconducting transition temperature of a small piece of tin, mounted together with the sample inside the pressure cell.

The pressure cell was further loaded into a low-temperature ^{3}He–^{4}He dilution refrigerator for transport and magnetic measurements down to $T = 0.06$ K. For both electrical resistivity and Hall measurements, a CePdAl sample of dimensions $0.2 \times 0.5 \times 2$ mm^3 was used; for magnetic susceptibility measurements, we employed a cube-like sample (~1 mm^3) cut from the same batch. The specific heat of nickel-doped samples was measured by a heat relaxation method employing a ^{3}He–^{4}He dilution refrigerator[24].

Data availability

The data that support the plots within this paper and other findings of this study are available from the corresponding author P.S. upon reasonable request.